THE JOURNAL OF PHYSICAL CHEMISTRY B

Article

pubs.acs.org/JPCB

Energetics of the S_2 State Spin Isomers of the Oxygen-Evolving Complex of Photosystem II

David J. Vinyard,[†,§] Sahr Khan,[‡,§] Mikhail Askerka, Victor S. Batista, and Gary W. Brudvig*

Department of Chemistry, Yale University, New Haven, Connecticut 06520-8107, United States

Supporting Information

ABSTRACT: The S_2 redox intermediate of the oxygen-evolving complex in photosystem II is present as two spin isomers. The S = 1/2 isomer gives rise to a multiline electron paramagnetic resonance (EPR) signal at g = 2.0, whereas the S = 5/2 isomer exhibits a broad EPR signal at g = 4.1. The electronic structures of these isomers are known, but their role in the catalytic cycle of water oxidation remains unclear. We show that formation of the S = 1/2 state from the S = 5/2 state is exergonic at temperatures above 160 K. However, the S = 1/2 isomer decays to S_1 more slowly than the S = 5/2 isomer. These differences support the hypotheses that the S_3 state is formed via the S_2 state S = 5/2 isomer and that the stabilized S_2 state S = 1/2 isomer plays a role in minimizing $S_2Q_A^-$ decay under light-limiting conditions.

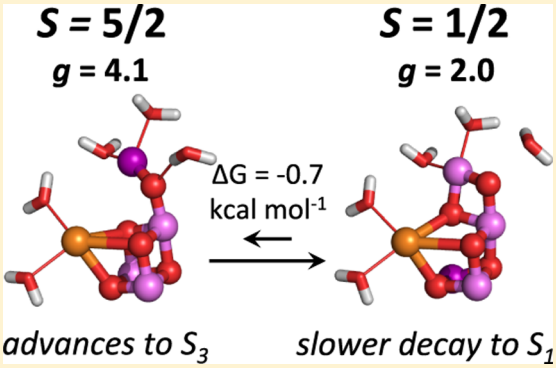

INTRODUCTION

In the catalytic cycle of the oxygen-evolving complex (OEC) of photosystem II (PSII), redox intermediates of the Mn_4CaO_5 complex are known as S_i states (i = 0−4).[1] In each turn of the S-state cycle, four oxidizing equivalents generated by photochemical charge separation events are used to oxidize two water molecules, forming one molecule of O_2 and reducing two molecules of plastoquinone to plastoquinol. Protons taken from the stroma and released into the lumen contribute to the transmembrane proton-motive force.[2]

The structure of the OEC in the dark-stable S_1 state has been determined using a combination of X-ray crystallography,[3,4] extended X-ray absorption fine structure (EXAFS) spectroscopy,[5,6] and quantum mechanical calculations.[7−10] Multiple lines of evidence (reviewed in ref 11) suggest that the S_1 state contains two Mn^{3+} and two Mn^{4+}. However, an alternative hypothesis asserts that the S_1 state contains either $(Mn^{3+})_4$ or $(Mn^{2+})(Mn^{3+})_2(Mn^{4+})$.[12,13]

The S_2 state is produced from the S_1 resting state by either continuous illumination at 130−220 K[14,15] or by a single-turnover flash at ambient temperature.[1,16] The S_2 state is paramagnetic and has been extensively studied using electron paramagnetic resonance (EPR) and EXAFS spectroscopy techniques.[17] No proton is released during the S_1 to S_2 transition, and one Mn ion is oxidized from Mn^{3+} to Mn^{4+}. The remaining Mn^{3+} center in the OEC in the S_2 state can be present at the Mn1 or Mn4 position (see Figure 1 for numbering). When Mn4 is Mn^{3+}, the OEC has a "closed cubane" motif and the ground spin state (S) is 5/2 (Figure 1A). When Mn1 is Mn^{3+}, the OEC is in an "open cubane" form and the ground spin state is 1/2 (Figure 1B).[9] The S = 5/2 spin isomer produces a nearly isotropic EPR signal at approximately g = 4.1,[14,18] whereas the S = 1/2 spin isomer produces a "multiline" EPR spectrum centered at g = 2.0 (Figure 1C).[16]

Both spin isomers are present in PSII membranes isolated from higher plants. However, the relative intensities of the two EPR signals (g = 4.1 and 2.0) are sensitive to experimental conditions, such as the illumination temperature and choice of cryoprotectant.[17] In native cyanobacterial PSII core complexes, only the S = 1/2 spin isomer is observed.

Whereas the electronic structures of the two S_2 spin isomers have been established by both experiment[21] and theory,[9] their relative energetics have not been established. Herein, we experimentally determine that the S = 1/2 isomer is approximately 0.7 kcal mol^{-1} more stable than the S = 5/2 isomer, consistent with quantum mechanics/molecular mechanics (QM/MM) calculations, and discuss the chemical mechanism of photosynthetic water oxidation in light of this finding.

METHODS

Spinach PSII membranes were prepared as previously described[22,23] and suspended to final chlorophyll concentrations of 5−8 mg mL^{-1} in 50 mM MES, 20 mM $Ca(OH)_2$, 10 mM NaCl, 0.01% Triton X-100, and 400 mM sucrose. The pH was adjusted to 6.0 with NaOH.

EPR spectra were recorded using a Bruker ELEXSYS E500 spectrometer, equipped with an SHQ cavity and Oxford ESR-900 helium flow cryostat, at 6−7 K. The instrument parameters were as follows: microwave frequency, 9.39 GHz; microwave power, 5 mW; modulation frequency, 100 kHz; modulation

Received: January 4, 2017
Published: January 12, 2017

DOI: 10.1021/acs.jpcb.7b00110
J. Phys. Chem. B 2017, 121, 1020−1025

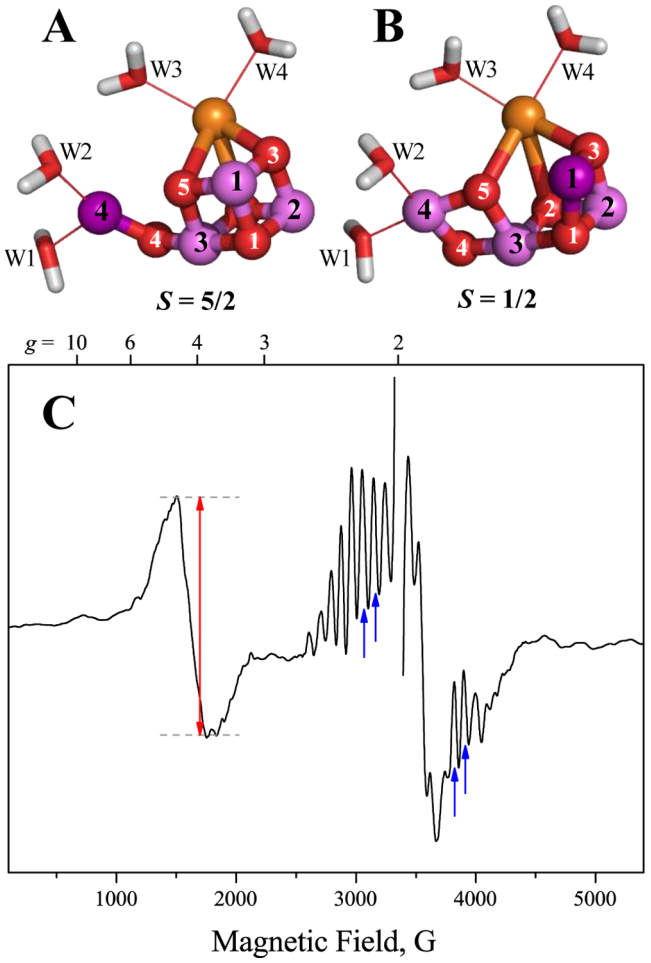

Figure 1. QM/MM optimized structures of the S_2 state spin isomers with ground states of $S = 5/2$ (A)[19] and $S = 1/2$ (B)[20] (see Pantazis et al.[9]). Mn^{3+} ions are shown in purple, Mn^{4+} in lavender, Ca^{2+} in orange, and O^{2-} in red. (C) The $S = 5/2$ isomer is characterized by a broad EPR signal at $g = 4.1$, and the $S = 1/2$ isomer gives rise to a multiline EPR signal centered at $g = 2.0$. The intensity of the $g = 4.1$ signal is measured as the peak-to-peak height, indicated by the red arrow. The intensity of the $g = 2.0$ signal is determined by summing the peak-to-peak heights of the four features indicated by blue arrows.

amplitude, 19.5 G; sweep time, 84 s; conversion time, 41 ms; time constant, 82 ms.

For S_2 state conversion experiments, 0.5 mM phenyl-*p*-benzoquinone (PPBQ) was added to each EPR sample from a 50 mM stock solution in dimethyl sulfoxide (DMSO). The EPR samples were illuminated in a quartz nitrogen flow cell at 135 K using a white xenon lamp supplemented with a near-IR light-emitting diode (LED; λ_{max} = 850 nm). After 4 min, the sample was quickly removed to liquid nitrogen (77 K) in darkness and transferred to the EPR cryostat. For incubations at <190 K, the sample was returned to the nitrogen flow cell. For incubations at ≥195 K, the sample was transferred to an equilibrated bath with varying ratios of ethanol/ethylene glycol in dry ice.

For $S_2Q_A^-$ decay experiments, 0.5 mM 3-(3,4-dichlorophenyl)-1,1-dimethylurea (DCMU) was added to each EPR sample from a 50 mM stock solution in DMSO. The EPR samples were illuminated in an ethanol/dry ice bath (200 K) using a white xenon lamp supplemented with a near-IR LED (λ_{max} = 850 nm). After 4 min, the sample was quickly removed to liquid nitrogen (77 K) in darkness and transferred to the EPR cryostat. For all incubations, the sample was transferred to an equilibrated bath of varying ratios of ethanol/ethylene glycol in dry ice.

For both experiments, incubations were performed in complete darkness and the temperature was continuously monitored using an external thermocouple.

EPR spectra subtractions and curve fittings were obtained using OriginPro 9.1. Temperature fluctuations during EPR measurements were ±0.1 K, leading to subtraction errors specifically in the $g \approx 4$ region due to rhombic iron contamination. These errors may affect EPR signal intensity measurements (Figure 1C) and are the predominant source of uncertainty in the values that we report. Nonlinear and linear curve fittings were performed in OriginPro using the Levenberg−Marquardt algorithm. Energy-minimized parameter values and associated standard errors are reported. For logarithmic plots, error bars span the natural logarithm of the mean ± standard error.

QM/MM calculations were performed as previously described,[8,19,20,24] using the B3LYP functional[25,26] with the LANL2DZ pseudopotential[27,28] for Ca and Mn and the 6-31G* basis set[29] for all other atoms for geometry optimizations and 6-311+G** for energy evaluations. The high layer and MM layer were chosen according to the scheme described in our previous models.[20] The AMBER force field was used for all MM layer atoms.[30]

RESULTS AND DISCUSSION

To study the kinetics of conversion of the $S = 5/2$ isomer to the $S = 1/2$ isomer, we illuminated dark-adapted PSII membranes isolated from spinach, containing the exogenous electron acceptor PPBQ and sucrose as a cryoprotectant, at 135 K. Under these conditions, only the $g = 4.1$ EPR signal is observed (Figure 2A)[14] because of the presence of near-IR light during illumination[31] (see Methods). After an initial EPR spectrum was obtained, the same sample was incubated in total darkness at 150−242 K, which led to conversion of the $g = 4.1$ to the $g = 2.0$ signal. For temperatures ≤170 K, the initial rate of conversion could be determined using this method (Figure 2B). Arrhenius analysis of the rate constants predicts an activation barrier of 6.7 ± 0.5 kcal mol^{-1} (Figure 2C). This barrier is in close agreement with that in a previous study by de Paula et al., who reported an activation barrier of 7.9 ± 1.4 kcal mol^{-1} for this conversion under similar conditions.[32]

For all tested temperatures, the $g = 4.1$ EPR signal decreased and the $g = 2.0$ EPR signal increased during dark incubation. This behavior has been previously reported by multiple groups.[14,31−33] The $g = 4.1$ signal intensity did not approach zero for extended incubation times (Figure 2A,B). Instead, the data suggest that a temperature-dependent equilibrium is established (see refs 31 and 34). For temperatures >170 K, the $g = 4.1$ signal decayed to a steady-state level in less than 300 s (first time point in Figure 2B). Although we could not determine the rates of S_2 state conversion in this temperature range due to fast conversion, equilibrium constants (defined here as $K_{eq} = [g = 2.0]/[g = 4.1]$) could be measured. As shown in Figure 3, K_{eq} is biphasic with respect to temperature. At temperatures <170 K, the van't Hoff treatment of the data provides a $\Delta H°$ of +31 kJ mol^{-1} and a $\Delta S°$ of +190 J mol^{-1} K^{-1}. At temperatures ≥195 K, the conversion of the $S = 5/2$ isomer to the $S = 1/2$ isomer is thermodynamically less demanding ($\Delta H°$ = +0.40 kJ mol^{-1} and $\Delta S°$ = +11 J mol^{-1}

DOI: 10.1021/acs.jpcb.7b00110
J. Phys. Chem. B 2017, 121, 1020−1025

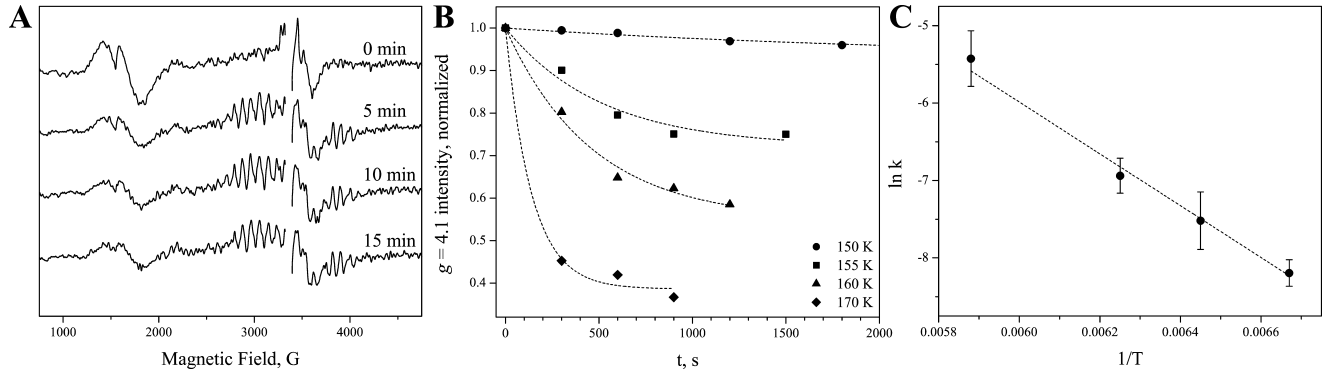

Figure 2. Kinetics of S_2 state conversion. (A) Only the g = 4.1 EPR signal is formed upon illumination at 135 K, as shown in the light − dark spectrum (top trace). During incubation in darkness at the representative temperature of 170 K in the presence of PPBQ, the g = 4.1 EPR signal decreases in intensity and the g = 2.0 EPR signal increases in intensity. Unsubtracted spectra are shown in Figure S1 of the Supporting Information. (B) Normalized peak-to-peak height of the g = 4.1 EPR signal vs. incubation time. Data were fit to a single exponential decay function ($y = y_0 + A\exp(-x/t)$) (dotted lines). (C) Arrhenius treatment of the data in (B). Error bars represent standard error of the fit. E_a = 6.7 ± 0.5 kcal mol^{-1}, A = 1.6 ± 0.2 × 10^6 s^{-1}, R^2 = 0.9867.

K^{-1}) and becomes exergonic for temperatures >160 K (Figure S2). When the data are extrapolated to 298 K, the equilibrium constant is estimated to be 3.2 ± 0.4, corresponding to ΔG° = −0.69 ± 0.14 kcal mol^{-1}.

The biphasic temperature dependence of the S_2 state spin isomer conversion may be caused by the surrounding protein environment. Extensive hydrogen-bonding networks involving water molecules, chloride, amino acid side chains, and the protein backbone amides surround the OEC and influence its properties.[35] For example, a second-shell water ligand, labeled Wx, is proposed to play a key role in water delivery to the OEC upon formation of the S_3 state.[19,36] As shown in Figure 4, Wx is a hydrogen-bond donor to the OEC in QM/MM structures of the S_1 state and the S_2 state S = 5/2 isomer. However, this hydrogen bond is broken upon formation of the S_2 state S = 1/2 isomer due to a dramatic decrease in the μ-oxo (O4) pK_a upon oxidation of Mn4 from Mn^{3+} to Mn^{4+}. We propose that the curvature in the data in Figure 3 reveals a 'glass transition' of the local environment around the OEC. At low temperatures, hydrogen-bonding interactions are frozen in place and only the S = 5/2 isomer can be formed from the S_1 state. However, at elevated temperatures above the glass-transition temperature, the hydrogen-bonding network can rearrange to accommodate the thermodynamically preferred S = 1/2 isomer. An H/D kinetic isotope effect of 2.5 associated with the conversion of the S_2 spin states at 160 K (Figure S3) further supports this hypothesis. Previous studies by Boussac and co-workers have shown that the g = 4.1 EPR signal formed by near-IR illumination at 77−160 K is different from the g = 4.1 EPR signal formed by 200 K illumination in terms of its temperature stability.[31,33,34,37] We propose that the changes in hydrogen-bonding networks above the observed glass transition may be responsible for this behavior.

To study the kinetics of decay of the $S_2Q_A^-$ state to the S_1Q_A state by charge recombination, dark-adapted PSII samples containing the secondary acceptor, Q_B site inhibitor DCMU, were illuminated at 200 K. Under these conditions, both the g = 4.1 and 2.0 EPR signals were observed (Figure 5A).[15] After an initial EPR spectrum was obtained, the same sample was incubated in total darkness at 218−258 K and the rates at which the g = 4.1 and 2.0 EPR signals decay were determined (Figure S4 in the Supporting Information). The g = 4.1 EPR signal was found to decay faster than the g = 2.0 signal.

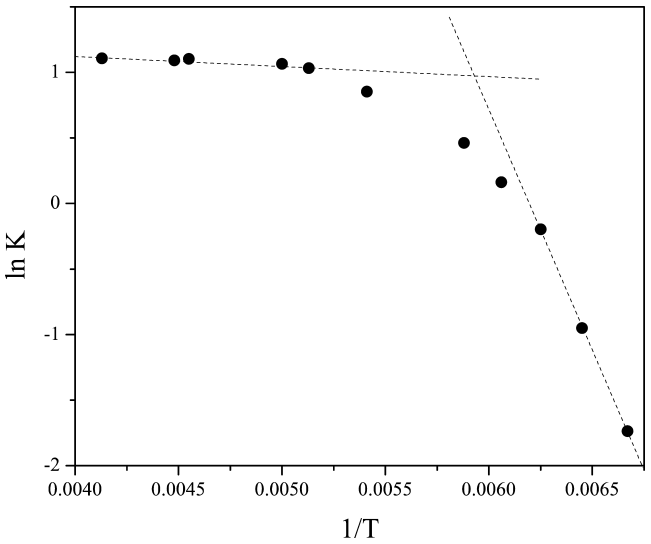

Figure 3. Temperature dependence of the equilibrium between S_2 states. van't Hoff treatment of K_{eq} (defined as [g = 2.0]/[g = 4.1]) shows two distinct linear regions. Fitted parameters are described in the text.

Arrhenius analysis of the rate constants provides an activation barrier for charge recombination of 6.3 ± 0.3 kcal mol^{-1} for the S_2 state g = 4.1 spin isomer and 10.5 ± 0.9 kcal mol^{-1} for the S_2 state g = 2.0 spin isomer (Figure 5B).

These experiments revealed two key energetic features of the S_2 state spin isomers: (1) conversion of the S = 5/2 isomer to the S = 1/2 isomer is exergonic at temperatures >160 K and (2) the S = 1/2 isomer has an activation barrier approximately 67% higher for charge recombination from $S_2Q_A^-$ to form S_1Q_A than that of the S = 5/2 isomer.

Several computational chemistry groups have estimated the relative energetics of the S_2 state spin isomers. Pantazis, Neese, and co-workers first used QM calculations to determine that the S = 1/2 isomer was more stable than the S = 5/2 isomer by 0.42−1.64 kcal mol^{-1}.[9] Similar results have been shown by Yamaguchi and co-workers (1.3 kcal mol^{-1})[38] and Kaila and co-workers (1.1 kcal mol^{-1}).[39] Guidoni et al. have used QM/MM−molecular dynamics methods to determine that the ΔG at 298 K between the S_2 state isomers is 1.1 kcal mol^{-1}, with

DOI: 10.1021/acs.jpcb.7b00110
J. Phys. Chem. B 2017, 121, 1020−1025

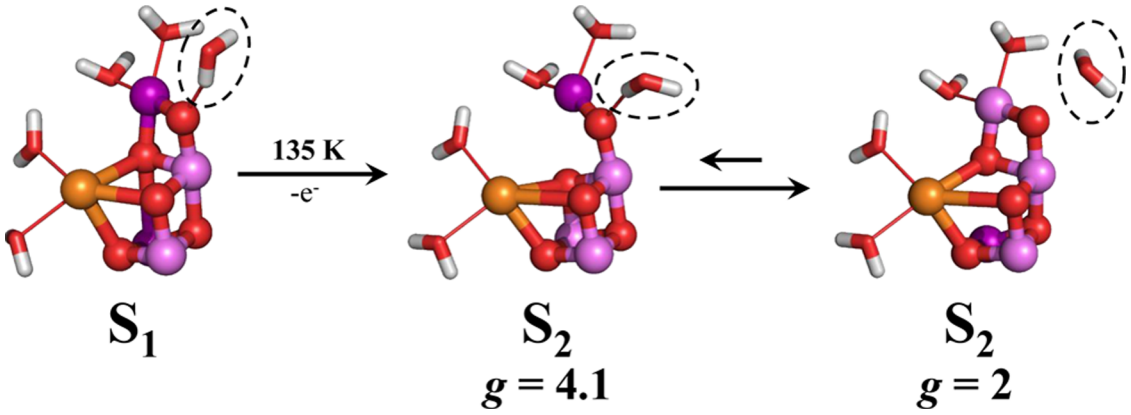

Figure 4. QM/MM optimized structures of the S_1 state and the two spin isomers of the S_2 state. Only the g = 4.1 EPR signal corresponding to the S = 5/2 spin isomer is formed at 135 K, but it spontaneously converts to the S = 1/2 spin isomer at temperatures >160 K. The second-shell water molecule, Wx, is circled in each structure. Wx is a hydrogen-bond donor to the OEC in the S_1 state and the S = 5/2 spin isomer of the S_2 state but not to the S = 1/2 spin isomer of the S_2 state. Mn^{3+} ions are shown in purple; Mn^{4+}, in lavender; Ca^{2+}, in orange; and O^{2-}, in red.

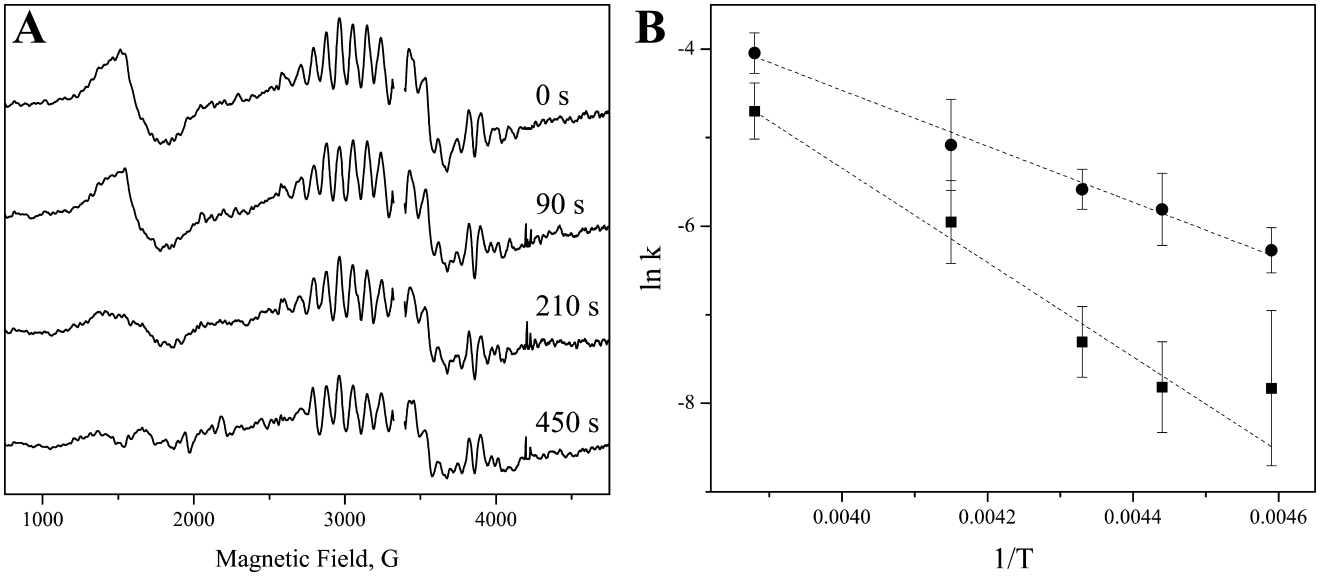

Figure 5. Kinetics of decay of $S_2Q_A^-$ to S_1Q_A. (A) Both the g = 4.1 and 2.0 EPR signals are formed upon illumination at 200 K, as shown in the light − dark spectrum (top trace). During incubation in darkness at the representative temperature of 218 K in the presence of DCMU, the g = 4.1 EPR signal decreases faster than the g = 2.0 EPR signal. Unsubtracted spectra are shown in Figure S5 of the Supporting Information. (B) Arrhenius analysis of the decay kinetics of $S_2Q_A^-$ to S_1Q_A. For the g = 4.1 EPR signal (circles), E_a = 6.3 ± 0.3 kcal mol^{-1}, A = 3.6 ± 0.3 × 10^3 s^{-1}, and R^2 = 0.9924. For the g = 2.0 EPR signal (squares), E_a = 10.5 ± 0.9 kcal mol^{-1}, A = 8.8 ± 1.1 × 10^6 s^{-1}, R^2 = 0.9699.

the S = 1/2 isomer being more stable.[40] Using QM/MM methods and the models described in the Methods, we find that the energy of the S = 1/2 isomer is 0.84 kcal mol^{-1} lower than that of the S = 5/2 isomer. All of these theoretical findings are in excellent agreement with the experimental results in this work (ΔG = −0.69 ± 0.14 kcal mol^{-1} at 298 K).

The kinetics of formation of the S_2 state and its conversion from the S = 1/2 spin isomer to the S = 5/2 spin isomer and vice versa have been harder to determine computationally, as the transition involves a change in both the spin state and geometry. The reaction barriers that we measure provide this vital information needed to delineate the PSII water-oxidation reaction coordinate.

These data suggest that in higher plant PSII at ambient temperature (298 K) approximately 75% of the S_2 state population is in the S = 1/2 spin isomer form, whereas approximately 25% is in the S = 5/2 spin isomer form. The excess S_2 state population in the S = 1/2 isomer form decays more slowly to S_1 via charge recombination with Q_A^-.

Previously, we and others have suggested that the S_3 state is formed via the S_2 state S = 5/2 isomer.[19,41] This seems to be in contradiction to the fact that the equilibrium between the S_2 spin isomers clearly favors the S = 1/2 isomer at 298 K. However, depending on environmental light conditions, cyanobacteria, algae, and plants must carefully balance the thermodynamics of OEC advancement and charge recombination.[42] The distribution of S_2 state spin isomers may thus play a role in regulating photosynthetic efficiency under light-limited conditions.[43] The majority of the S_2 state population remains in the stabilized low-spin isomer form that has a slower $S_2Q_A^-$ charge recombination. A minority of the S_2 state population is in the reactive high-spin isomer form that has a faster $S_2Q_A^-$ charge recombination but can advance to the S_3 state. Balancing these two populations can thus tune the overall efficiency of PSII. Pantazis and co-workers and Guidoni and co-workers

DOI: 10.1021/acs.jpcb.7b00110
J. Phys. Chem. B 2017, 121, 1020−1025

have used computational methods to show that the relative S_2 spin isomer populations change when Y_Z is oxidized.[41,44] Although the influence of Y_Z is outside the scope of this study, it is likely an important factor in the S_2 to S_3 transition.

CONCLUSIONS

We have determined the energetics of the S_2 state spin isomers (summarized in Figure 6). The S_2 state spin isomer conversion

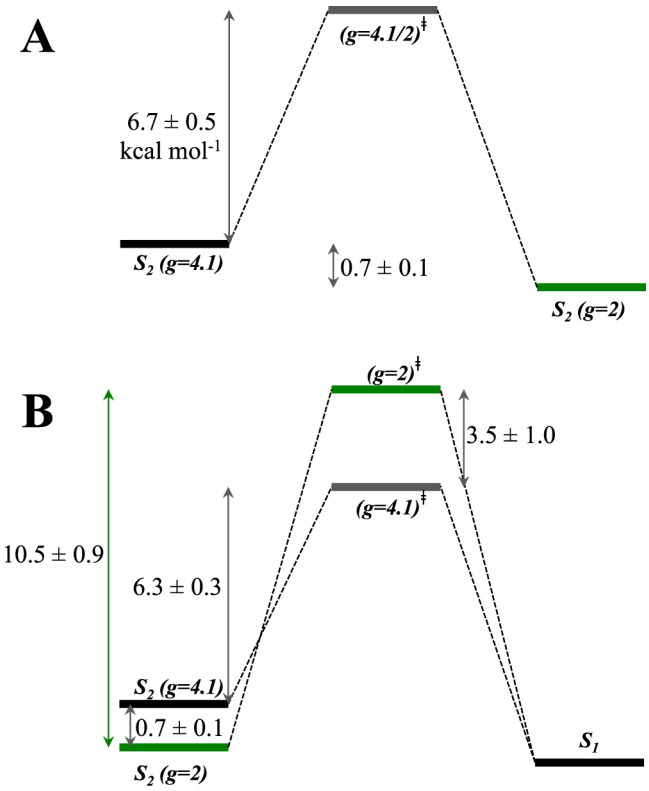

Figure 6. Compiled energetics schemes for the (A) conversion of the S_2 state $S = 5/2$ isomer to the S_2 state $S = 1/2$ isomer and (B) decay of the $S_2Q_A^-$ state to S_1Q_A for both S_2 state spin isomers. The double dagger symbol denotes a transition state.

experiments reveal that the free-energy difference between the two ground spin states is 0.69 ± 0.14 kcal mol^{-1} at 298 K, with the $S = 1/2$ spin isomer being more stable. $S_2Q_A^-$ decay experiments reveal that the $S = 5/2$ spin isomer has a lower activation barrier for charge recombination to form S_1Q_A than the $S = 1/2$ spin isomer. These differences support the hypotheses that the S_3 state is formed from the S_2 state $S = 5/2$ spin isomer and that the stabilized S_2 state $S = 1/2$ spin isomer plays a role in minimizing $S_2Q_A^-$ decay under light-limiting conditions. These findings provide experimental insights into the mechanism of natural water oxidation.

ASSOCIATED CONTENT

Supporting Information

The Supporting Information is available free of charge on the ACS Publications website at DOI: 10.1021/acs.jpcb.7b00110.

Figures showing unsubtracted EPR spectra for Figures 2A and 5A and temperature dependence of the free energy of S_2 state spin isomer conversion, S_2 state spin isomer conversion in D_2O, and $S_2Q_A^-$ decay data at 218−258 K (PDF)

AUTHOR INFORMATION

Corresponding Author

*E-mail: gary.brudvig@yale.edu. Phone: (203) 432-5202. Fax: (203) 432-6144.

ORCID

Victor S. Batista: 0000-0002-3262-1237

Gary W. Brudvig: 0000-0002-7040-1892

Present Addresses

†Department of Biological Sciences, Louisiana State University, Baton Rouge, Louisiana 70803, United States (D.J.V.).

‡Department of Chemistry, Massachusetts Institute of Technology, Cambridge, Massachusetts 02139, United States (S.K.).

Author Contributions

§D.J.V and S.K. contributed equally.

Notes

The authors declare no competing financial interest.

ACKNOWLEDGMENTS

The authors acknowledge the support by the U.S. Department of Energy, Office of Science, Office of Basic Energy Sciences, Division of Chemical Sciences, Geosciences, and Biosciences, Photosynthetic Systems. The experimental work was funded by Grant DE-FG02-05ER15646 (G.W.B.), and the computational work was funded by Grant DESC0001423 (V.S.B). We thank the National Energy Research Scientific Computing Center (NERSC) and Shanghai Jiao Tong University II High Performance Computation Center for generous computer time allocations. We thank Prof. Marilyn Gunner for helpful discussions.

REFERENCES

(1) Kok, B.; Forbush, B.; McGloin, M. Cooperation of charges in photosynthetic O_2 evolution I. A linear four step mechanism. *Photochem. Photobiol.* **1970**, *11*, 457−475.

(2) Blankenship, R. E. *Molecular Mechanisms of Photosynthesis*, 2nd ed.; John Wiley & Sons, Ltd.: Chichester, 2014.

(3) Umena, Y.; Kawakami, K.; Shen, J.-R.; Kamiya, N. Crystal structure of oxygen-evolving photosystem II at a resolution of 1.9 Å. *Nature* **2011**, *473*, 55−60.

(4) Suga, M.; Akita, F.; Hirata, K.; Ueno, G.; Murakami, H.; Nakajima, Y.; Shimizu, T.; Yamashita, K.; Yamamoto, M.; Ago, H.; et al. Native structure of photosystem II at 1.95 Å resolution viewed by femtosecond X-ray pulses. *Nature* **2014**, *517*, 99−103.

(5) Grundmeier, A.; Dau, H. Structural models of the manganese complex of photosystem II and mechanistic implications. *Biochim. Biophys. Acta, Bioenerg.* **2012**, *1817*, 88−105.

(6) Sauer, K.; Yano, J.; Yachandra, V. K. X-ray spectroscopy of the photosynthetic oxygen-evolving complex. *Coord. Chem. Rev.* **2008**, *252*, 318−335.

(7) Luber, S.; Rivalta, I.; Umena, Y.; Kawakami, K.; Shen, J.-R.; Kamiya, N.; Brudvig, G. W.; Batista, V. S. S_1-state model of the O_2-evolving complex of photosystem II. *Biochemistry* **2011**, *50*, 6308−6311.

(8) Pal, R.; Negre, C. F. A.; Vogt, L.; Pokhrel, R.; Ertem, M. Z.; Brudvig, G. W.; Batista, V. S. S_0-state model of the oxygen-evolving complex of photosystem II. *Biochemistry* **2013**, *52*, 7703−7706.

(9) Pantazis, D. A.; Ames, W.; Cox, N.; Lubitz, W.; Neese, F. Two interconvertible structures that explain the spectroscopic properties of the oxygen-evolving complex of photosystem II in the S_2 state. *Angew. Chem., Int. Ed. Engl.* **2012**, *51*, 9935−9940.

(10) Siegbahn, P. E. M. Water oxidation mechanism in photosystem II, including oxidations, proton release pathways, O−O bond formation and O_2 release. *Biochim. Biophys. Acta, Bioenerg.* **2013**, *1827*, 1003−1019.

DOI: 10.1021/acs.jpcb.7b00110
J. Phys. Chem. B 2017, 121, 1020−1025

(11) Vinyard, D. J.; Khan, S.; Brudvig, G. W. Photosynthetic water oxidation: Binding and activation of substrate waters for O−O bond formation. *Faraday Discuss.* **2015**, *185*, 37−50.
(12) Vinyard, D. J.; Ananyev, G. M.; Dismukes, G. C. Photosystem II: The reaction center of oxygenic photosynthesis. *Annu. Rev. Biochem.* **2013**, *82*, 577−606.
(13) Gatt, P.; Petrie, S.; Stranger, R.; Pace, R. J. Rationalizing the 1.9 Å crystal structure of photosystem II—A remarkable Jahn−Teller balancing act induced by a single proton transfer. *Angew. Chem., Int. Ed.* **2012**, *51*, 12025−12028.
(14) Casey, J. L.; Sauer, K. EPR detection of a cryogenically photogenerated intermediate in photosynthetic oxygen evolution. *Biochim. Biophys. Acta, Bioenerg.* **1984**, *767*, 21−28.
(15) de Paula, J. C.; Innes, J. B.; Brudvig, G. W. Electron transfer in photosystem II at cryogenic temperatures. *Biochemistry* **1985**, *24*, 8114−8120.
(16) Dismukes, G. C.; Siderer, Y. Intermediates of a polynuclear manganese center involved in photosynthetic oxidation of water. *Proc. Natl. Acad. Sci. U.S.A.* **1981**, *78*, 274−278.
(17) Pokhrel, R.; Brudvig, G. W. Oxygen-evolving complex of photosystem II: Correlating structure with spectroscopy. *Phys. Chem. Chem. Phys.* **2014**, *16*, 11812−11821.
(18) Zimmermann, J. L.; Rutherford, A. W. Electron paramagnetic resonance properties of the S_2 state of the oxygen-evolving complex of photosystem II. *Biochemistry* **1986**, *25*, 4609−4615.
(19) Askerka, M.; Vinyard, D. J.; Brudvig, G. W.; Batista, V. S. NH_3 binding to the S_2 state of the O_2-evolving complex of photosystem II: Analogue to H_2O binding during the $S_2 \rightarrow S_3$ transition. *Biochemistry* **2015**, *54*, 5783−5786.
(20) Askerka, M.; Wang, J.; Brudvig, G. W.; Batista, V. S. Structural changes in the oxygen-evolving complex of photosystem II induced by the S_1 to S_2 transition: A combined XRD and QM/MM study. *Biochemistry* **2014**, *53*, 6860−6862.
(21) Chatterjee, R.; Han, G.; Kern, J.; Gul, S.; Fuller, F. D.; Garachtchenko, A.; Young, I. D.; Weng, T.-C.; Nordlund, D.; Alonso-Mori, R.; et al. Structural changes correlated with magnetic spin state isomorphism in the S_2 state of the Mn_4CaO_5 cluster in the oxygen-evolving complex of photosystem II. *Chem. Sci.* **2016**, *7*, 5236−5248.
(22) Berthold, D. A.; Babcock, G. T.; Yocum, C. F. A highly resolved, oxygen-evolving photosystem II preparation from spinach thylakoid membranes. *FEBS Lett.* **1981**, *134*, 231−234.
(23) Beck, W. F.; de Paula, J. C.; Brudvig, G. W. Active and resting states of the oxygen-evolving complex of photosystem II. *Biochemistry* **1985**, *24*, 3035−3043.
(24) Askerka, M.; Vinyard, D. J.; Wang, J.; Brudvig, G. W.; Batista, V. S. Analysis of the radiation-damage-free X-ray structure of photosystem II in light of EXAFS and QM/MM data. *Biochemistry* **2015**, *54*, 1713−1716.
(25) Becke, A. D. Density-functional exchange-energy approximation with correct asymptotic behavior. *Phys. Rev. A* **1988**, *38*, 3098−3100.
(26) Becke, A. D. Density-functional thermochemistry. III. The role of exact exchange. *J. Chem. Phys.* **1993**, *98*, 5648−5652.
(27) Hay, P. J.; Wadt, W. R. Ab initio effective core potentials for molecular calculations. Potentials for K to Au including the outermost core orbitals. *J. Chem. Phys.* **1985**, *82*, 299−310.
(28) Wadt, W. R.; Hay, P. J. Ab initio effective core potentials for molecular calculations. Potentials for main group elements Na to Bi. *J. Chem. Phys.* **1985**, *82*, 284−298.
(29) Hariharan, P. C.; Pople, J. A. The influence of polarization functions on molecular orbital hydrogenation energies. *Theoret. Chim. Acta* **1973**, *28*, 213−222.
(30) Case, D. A.; Darden, T. A.; Cheatham, T. E.; Simmerling, C. L.; Wang, J.; Duke, R. E.; Luo, R.; Walker, R. C.; Zhang, W.; Merz, K. M.; et al. *AMBER 12*; University of California: San Francisco, 2012.
(31) Boussac, A.; Girerd, J.-J.; Rutherford, A. W. Conversion of the spin state of the manganese complex in photosystem II induced by near-infrared light. *Biochemistry* **1996**, *35*, 6984−6989.
(32) de Paula, J. C.; Beck, W. F.; Miller, A.-F.; Wilson, R. B.; Brudvig, G. W. Studies of the manganese site of photosystem II by electron spin resonance spectroscopy. *J. Chem. Soc., Faraday Trans. 1* **1987**, *83*, 3635−3651.
(33) Boussac, A.; Un, S.; Horner, O.; Rutherford, A. W. High-spin states ($S \geq 5/2$) of the photosystem II manganese complex. *Biochemistry* **1998**, *37*, 4001−4007.
(34) Boussac, A.; Rutherford, A. W. Comparative study of the g = 4.1 EPR signals in the S_2 state of photosystem II. *Biochim. Biophys. Acta, Bioenerg.* **2000**, *1457*, 145−156.
(35) Vogt, L.; Vinyard, D. J.; Khan, S.; Brudvig, G. W. Oxygen-evolving complex of photosystem II: An analysis of second-shell residues and hydrogen-bonding networks. *Curr. Opin. Chem. Biol.* **2015**, *25*, 152−158.
(36) Capone, M.; Narzi, D.; Bovi, D.; Guidoni, L. Mechanism of water delivery to the active site of photosystem II along the S_2 to S_3 transition. *J. Phys. Chem. Lett.* **2016**, *7*, 592−596.
(37) Boussac, A.; Sugiura, M.; Kirilovsky, D.; Rutherford, A. W. Near-infrared-induced transitions in the manganese cluster of photosystem II: Action spectra for the S_2 and S_3 redox states. *Plant Cell Physiol.* **2005**, *46*, 837−842.
(38) Isobe, H.; Shoji, M.; Shen, J.-R.; Yamaguchi, K. Strong coupling between the hydrogen bonding environment and redox chemistry during the S_2 to S_3 transition in the oxygen-evolving complex of photosystem II. *J. Phys. Chem. B* **2015**, *119*, 13922−13933.
(39) Ugur, I.; Rutherford, A. W.; Kaila, V. R. I. Redox-coupled substrate water reorganization in the active site of photosystem II—The role of calcium in substrate water delivery. *Biochim. Biophys. Acta, Bioenerg.* **2016**, *1857*, 740−748.
(40) Bovi, D.; Narzi, D.; Guidoni, L. The S_2 state of the oxygen-evolving complex of photosystem II explored by QM/MM dynamics: Spin surfaces and metastable states suggest a reaction path towards the S_3 state. *Angew. Chem., Int. Ed. Engl.* **2013**, *52*, 11744−11749.
(41) Retegan, M.; Krewald, V.; Mamedov, F.; Neese, F.; Lubitz, W.; Cox, N.; Pantazis, D. A. A five-coordinate Mn(IV) intermediate in biological water oxidation: spectroscopic signature and a pivot mechanism for water binding. *Chem. Sci.* **2016**, *7*, 72−84.
(42) Rutherford, A. W.; Osyczka, A.; Rappaport, F. Back-reactions, short-circuits, leaks and other energy wasteful reactions in biological electron transfer: Redox tuning to survive life in O_2. *FEBS Lett.* **2012**, *586*, 603−616.
(43) Krewald, V.; Retegan, M.; Neese, F.; Lubitz, W.; Pantazis, D. A.; Cox, N. Spin state as a marker for the structural evolution of nature's water-splitting catalyst. *Inorg. Chem.* **2016**, *55*, 488−501.
(44) Narzi, D.; Bovi, D.; Guidoni, L. Pathway for Mn-cluster oxidation by tyrosine-Z in the S_2 state of photosystem II. *Proc. Natl. Acad. Sci. U.S.A.* **2014**, *111*, 8723−8728.

DOI: 10.1021/acs.jpcb.7b00110
J. Phys. Chem. B 2017, 121, 1020−1025